

INVESTIGATION OF THE EFFECT OF RADIATION ON THE THERMOPHORETIC  
MOTION OF SOOT PARTICLES IN FREE—MOLECULAR REGIME

Except where reference is made to the work of others, the work described in this thesis is my own or was done in collaboration with my advisory committee. This thesis does not include proprietary or classified information.

---

Vamshi Krishna Sarangapani

Certificate of Approval:

---

Jay M. Khodadadi  
Professor  
Mechanical Engineering

---

Daniel W. Mackowski, Chair  
Associate Professor  
Mechanical Engineering

---

Daniel K. Harris  
Associate Professor  
Mechanical Engineering

---

Stephen L. McFarland  
Acting Dean  
Graduate School

INVESTIGATION OF THE EFFECT OF RADIATION ON THE THERMOPHORETIC  
MOTION OF SOOT PARTICLES IN FREE—MOLECULAR REGIME

Vamshi Krishna Sarangapani

A Thesis  
Submitted to  
the Graduate Faculty of  
Auburn University  
in Partial Fulfillment of the  
Requirements for the  
Degree of  
Master of Science

Auburn, Alabama

August 08, 2005

INVESTIGATION OF THE EFFECT OF RADIATION ON THE THERMOPHORETIC  
MOTION OF SOOT PARTICLES IN FREE—MOLECULAR REGIME

Vamshi Krishna Sarangapani

Permission is granted to Auburn University to make copies of this thesis at its discretion, upon the request of individuals or institutions and at their expense.  
The author reserves all publication rights.

---

Signature of Author

---

Date

Copy sent to:

Name

Date

## VITA

Vamshi Krishna Sarangapani, son of Venkataramana Chary Sarangapani and Ramadevi Sarangapani, was born on August 12, 1980, in Dharmapuri, Andhra Pradesh, India. He graduated with the degree of Bachelor of Technology in Mechanical Engineering in 2003 from Indian Institute of Technology, Madras, India. He joined the Masters program in the department of Mechanical Engineering at Auburn University in August 2003.

THESIS ABSTRACT

INVESTIGATION OF THE EFFECT OF RADIATION ON THE THERMOPHORETIC  
MOTION OF SOOT PARTICLES IN FREE—MOLECULAR REGIME

Vamshi Krishna Sarangapani

Master of Science, August 08, 2005  
(B.Tech., Indian Institute of Technology, Madras, India. June 2003)

68 Typed Pages

Directed by Daniel W. Mackowski

The coupling of radiation and thermophoresis is hypothesized to result in attractive forces among soot particles in combustion environments. The effect of radiation from the soot particles on their thermophoretic motion in the free—molecular regime is studied by developing a ‘synthetic’ simulation model. A Monte Carlo technique is used to carry out this study and the models are developed both for the two—particle system and the aggregate system that mimics cluster—cluster aggregation. The transfer of momentum and energy to and from the soot particles are computed via the monte carlo method. The thermophoretic force and the coagulation ratios are calculated for the developed models. The results indicate that thermophoresis would be a significant mode of soot particle coagulation for larger particle sizes and higher gas temperatures. The sphere aggregates are compared to single spheres with equivalent volume, surface area, and radius of gyration and the results show that the aggregate can be approximated to its volume equivalent sphere in a two—sphere model.

## ACKNOWLEDGMENTS

I would like to thank my advisor, Professor Daniel W. Mackowski for his constant support and guidance throughout my research at Auburn University and providing me with an opportunity to work in this exciting field. His methodology has greatly helped me hone the thought process that goes into approaching and solving a problem. I would also like to thank Professors Jay M. Khodadadi and Daniel K. Harris for serving on my graduate committee. I thank all the professors, staff, and students I have had interactions with throughout this study. Finally, I thank all my friends for their help and support when I needed them the most.

I wish to dedicate this work to my parents and my younger brother whose love and encouragement provide me the strength to sail through life and achieve my goals.

Style manual or journal used *L<sup>A</sup>T<sub>E</sub>X* – A Document Preparation System, Leslie Lamport, *Addison-Wesley Publishing Company*, 2nd edition (1994). Bibliography follows *IEEE Transactions*.

---

Computer software used The document preparation package T<sub>E</sub>X (specifically L<sup>A</sup>T<sub>E</sub>X) together with the departmental style-file `aums.sty`. The plots were generated using *MATLAB*<sup>®</sup>.

---

## TABLE OF CONTENTS

LIST OF FIGURES		x
LIST OF TABLES		xi
1	INTRODUCTION	1
1.1	Motivation . . . . .	1
1.2	Hypothesis . . . . .	3
1.3	Objectives . . . . .	3
1.4	Thesis Statement . . . . .	5
2	LITERATURE REVIEW	6
2.1	Experimental Approach . . . . .	6
2.2	Simulation Model . . . . .	7
2.2.1	Soot Aggregates . . . . .	7
2.2.2	Thermophoresis . . . . .	8
2.2.3	Knudsen Number . . . . .	9
3	THE MODEL	12
3.1	The velocity distribution function . . . . .	12
3.2	Sampling of the distribution function . . . . .	15
3.3	The two sphere model . . . . .	17
3.3.1	Energy transport . . . . .	19
3.3.2	Momentum transfer . . . . .	22
3.3.3	Soot radiation heat source function . . . . .	23
3.3.4	Thermophoretic force analysis . . . . .	27
3.3.5	Monte Carlo method . . . . .	29
3.4	Aggregate model . . . . .	32
3.4.1	Modified Monte Carlo method . . . . .	32
4	RESULTS AND CONCLUSIONS	35
4.1	Results . . . . .	35
4.1.1	The two sphere model . . . . .	35
4.1.2	Aggregate model . . . . .	36
4.1.3	Two-sphere equivalent of aggregate model . . . . .	41
4.1.4	Coagulation ratio . . . . .	42
4.2	Conclusions . . . . .	43
4.3	Suggestions for future research . . . . .	44



BIBLIOGRAPHY	46
APPENDICES	48
A MONTE CARLO CODE FOR THE TWO-SPHERE MODEL	49
B MONTE CARLO CODE FOR THE AGGREGATE MODEL	52

## LIST OF FIGURES

1.1	TEM photograph of a soot aggregate . . . . .	4
3.1	Two-sphere model showing the ray trace of a molecule . . . . .	18
3.2	Soot aggregate generated using the power law . . . . .	33
3.3	Aggregate-model showing the ray trace of a molecule . . . . .	34
4.1	Two sphere model – Force vs Distance . . . . .	36
4.2	Log-Log scale of Fig.4.1 . . . . .	37
4.3	$F_{1-cluster}$ vs $N_{samp}$ . . . . .	38
4.4	Aggregate model – Force vs Distance . . . . .	39
4.5	Log-Log scale of Fig.4.4 . . . . .	40

LIST OF TABLES

4.1	Comparison of thermophoretic force magnitudes . . . . .	41
4.2	Coagulation ratios for various $a$ and $T$ . . . . .	43
4.3	Coagulation ratios for various $a$ and $T$ . . . . .	43

## CHAPTER 1

### INTRODUCTION

#### 1.1 Motivation

Combustion plays an important role in automobile industry, industrial burners and furnaces, gas turbines, etc., as the process involves conversion of chemical energy in fuels to thermal energy that generates power. In addition to playing a helpful role, combustion processes also have detrimental affects on the human lives in the form of harmful emissions such as  $NO_x$ , and soot. Soot is formed in gas-phase combustion at high temperature. At the microscopic level, soot forms when hydrocarbons are heated with insufficient air due to poor mixing. In flames, soot can be observed in diffusion flames as opposed to premixed flames, where a clean blue flame can be seen. Keeping in view the importance of soot, its study has been a major area of interest for quite some time now. In boilers, soot fouling is a big concern as it brings down the efficiency. Soot is suspended in air and because of its extremely small size, penetrates deep in to the lungs, thus affecting our respiratory system. In some devices, such as furnaces, the thermal emission from soot enhances heat transfer process via radiation. Soot is also an important industrial product that finds application, such as filler in tires, toner in copiers, etc..

Soot collected from flames consists of chain-like aggregates of spherical units. These spherical units have a hexagonal structure similar to graphite [1], and the sizes range between 10 nm and 80 nm. Soot formation is believed to take place in three steps: [1] Particle inception or Nucleation: this step involves a series of homogenous

reactions between hydrocarbon species leading to a larger sized particles which can be seen under an electron microscope as tiny spherical condensed particles [2]. The rate of particle inception is extremely high, though the particles formed in this step constitute only a minor fraction of the final soot mass. (2) Surface Growth: in this step, two processes are believed to occur simultaneously. First, the small spherical particles formed in step [1] collide and coalesce to form larger spheres. Second, the hydrocarbon “growth species” in the gas phase react heterogeneously on the soot surfaces [2]. (3) Aggregation: the spherical particles formed in step-(2) collide and stick (but they no longer coalesce) to form chains. The soot formed can be controlled only by Oxidation. It is the sole mechanism of removal of soot emission. In this process, the soot particles formed are changed back into gas-phase species.

While soot is a major pollutant, it is an important industrial product and is a major source of radiation from flames. In most of the hydrocarbon fuels combustion, the dominant part of radiation comes from the soot particles. The fourth power dependence on temperature also makes radiation a prime mode of heat transfer in most flames. Radiation allows transfer of energy directly from hot product regions to cold regions, exerting its effects even at a distance.

Modelling of the formation, growth, and deposition of soot requires an understanding of the mechanisms which transport the soot in a gas. These mechanisms include convection, diffusion, sedimentation, and thermophoresis. A significant transport of soot in flames is by thermophoresis. The term 'thermophoresis' is given to the motion of aerosol particles that move, with a constant velocity, towards lower temperature regions, under the influence of a temperature gradient. Thermophoresis

occurs because the momentum carried by the hot gas molecules that sink the particles is greater than that carried by the particles coming from cold region. Studies have confirmed that thermophoresis results in a larger deposition rate of aerosols than either of sedimentation or diffusion processes [3].

## **1.2 Hypothesis**

It can be observed, in flames, that when a steel rod which is at room temperature is introduced, the soot particles get deposited at a quick rate on that rod. This behavior is observed as a result of thermophoresis. The temperature gradient existing between the emanating soot particles and the steel rod causes the movement of the particles towards the rod. It is submitted that a similar effect can occur among the soot particles themselves. As a result of continuous radiation from the soot particles, the local temperature of the gas is affected resulting in temperature gradients. These temperature gradients lead to an attractive thermophoretic motion among the soot particles. The objective of this thesis is to carry out investigations on the effect of radiation from soot particles on the thermophoretic motion of the soot particles, and establish that the coupling of radiation and thermophoresis could result in attractive forces among soot particles.

## **1.3 Objectives**

The goal of this thesis can be achieved either by investigating the process experimentally or by building a simulation model. There may be some practicalities, in studying the process by building an experimental set-up, such as low residence

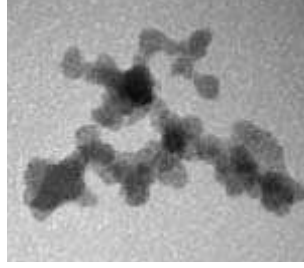


Figure 1.1: TEM photograph of a soot aggregate

times. Likewise, building a simulation model of the effect of soot radiation on the thermophoretic motion of the particles is a complicated one because of the 3-D nature of the problem. Nevertheless, the complexity can be reduced if we initially build a simulation model for a simple system. Therefore, the initial step would be to model a simple system of soot particles, essentially, a two-particle model. Extension of this model to a more general system of particles could be carried out at a later stage. In order to get started, even with the simplest of cases, we need to make some basic assumptions. First among those would be the shape of the soot particles we are simulating. Transmission Electron Microscopy (TEM) measurements indicate that soot aggregates consist of nearly spherical primary particles. Figure 1.1 is a TEM image of a typical soot aggregate found within the annular region of a diffusion flame [15]. The measurements show that the aggregates exhibit mass fractal behavior. The flame generated soot aggregates exhibit mass fractal-like behavior with a fractal dimension,  $D_f < 2$ , even when the number of primary particles in an aggregate is small [4]. The second assumption would be the size of the particles. The soot particles we consider would be nearly nano-sized, making them considerably smaller than the mean free path. This assumption is supported by the gas temperatures we would be dealing

with ( $\sim 1500\text{ K}$ ). At such high temperatures, the mean free path increases, thus justifying our assumption of knudsen number,  $Kn \gg 1$  (i.e., the mean free path  $\gg$  the particle size).

#### 1.4 Thesis Statement

This thesis consists broadly of two parts: the first part discusses the effect of radiation on the thermophoretic motion between two primary aerosol particles (assumed to be spheres), and the second part discusses the effect of radiation on the thermophoretic motion between a cluster and a single particle.

This thesis is organized as follows: Chapter 2 gives a more detailed description of the work done in the area of interest and the existing methodologies (literature review). Chapter 3 presents details of the proposed methodology and the algorithm employed. Chapter 4 presents the results of the proposed method and various observations that can be drawn from those results. Chapter 4 also includes suggestions for future research.



## CHAPTER 2

### LITERATURE REVIEW

#### 2.1 Experimental Approach

The main aim of the experimental approach is to visually observe the coagulation of soot particles as a result of the proposed hypothesis. Studies were previously carried to observe this effect using co-flow diffusion burners. As a result of low residence times, it was difficult to keep the soot particles for sufficient time in the flame environment. Burner assemblies that offer longer residence times than those possible in the co-flow diffusion burner assembly were looked in for from the available literature. A flat counter-flow diffusion burner assembly that offers longer residence time was then built in the laboratory. A flat counter-flow diffusion flame was established using methane as the fuel. Nitrogen was the inert gas used. The study with this assembly was also inconclusive, mainly because of two factors. The first factor was again the low residence time (we obtained longer residence time than in the case of co-flow diffusion flame, but not good enough to observe the effect). The order of residence time we obtained was about 1s. The second factor is that the gelation process was overpowering all the other effects, making it difficult to observe the intended process. Once the aggregate size reaches a large value, the aggregation of soot particles is largely because of the gelation effect. The soot cloud forms a sort of “spider-web,” thereby attracting the soot particles to stick to the cloud. This is the effect we primarily notice if we run an experiment, thus making the study of effect of radiation on thermophoretic motion of soot particles inconclusive.

## 2.2 Simulation Model

Taking into consideration the practicalities in running an experiment, we opted for a simulation model. The subsequent sections in this chapter discuss briefly on soot aggregates and thermophoresis.

### 2.2.1 Soot Aggregates

Computer simulations were carried out to develop models for random cluster formation by researchers [5,6] since early 80's. Sorensen, in his paper discusses about various aggregation algorithms for simulating aggregates [7] using the power law,

$$N = K_0(R_g/a)^{D_f} \quad (2.1)$$

Where  $N$  is the number of monomers in the aggregate,  $R_g$  is the radius of gyration,  $a$  is the monomer radius,  $D_f$  is the fractal dimension, and the proportionality constant  $K_0$  is the prefactor. In [7], random aggregates have been computer synthesized using both Diffusion Limited Aggregation (DLA) and Diffusion Limited Cluster Aggregation (DLCA).

In DLA, a monomer is chosen from a set of  $N$  monomers and placed at the center of the sphere. The second monomer is now brought near the first and random-walked until it is attached at a random angular position. Subsequent monomers are then introduced one-by-one at a random angular position.

In DLCA, two monomers are chosen at random from a set of  $N$ ; one of them is placed at the center and the second one is introduced at a random angular position,

random-walked around the first one. This cluster is now put back into the set if the pair of monomers are joined making the set, now,  $(N-1)$  long. The process is repeated to obtain the desired length of cluster.

A plot of  $\log(N)$  vs  $\log(R_g)$  will produce a straight line with slope  $D_f$  and y-intercept  $K_0$ .

### 2.2.2 Thermophoresis

Since its discovery, numerous applications have been recognized where thermophoresis can play either positive or adverse roles [8]. Principle of thermophoresis has been extensively used in the design of thermal precipitators, and aerosol sampling methods. Thermophoresis can result in particle deposition on boiler pipes, reducing the efficiency of heat exchange. The effect of thermophoresis on the transfer of the radioactive aerosols generated in a nuclear reactor accident has been recognized as an important factor in reactor safety assessment. The principle of thermophoresis can be used to enhance chemical vapor deposition process which is a key in fabrication of optical fibers. It has been used as an effective method for micro-contamination control in the semiconductor industry [8]. Application areas of effect of thermophoresis also include: aerosol instruments and devices, microelectronics, xerography, drug delivery and pharmaceutical, and atmospheric dispersion.

Let us now see why thermophoresis occurs. At the molecular level, the gas molecules coming from the hot region carry more momentum than those moving from the cold region. This imbalance results in a net force from hot region to a cold

region. It should also be noted that the entire imbalance in momentum transfer is only because of the incoming flux of molecules. The re-emission of molecules (outward flux) is assumed to be *diffuse* because of the perfect accommodation of spheres (soot particles). Thermophoretic force can be determined by solving momentum transfer and energy transfer equations using the distribution functions. These distribution functions are governed by the Boltzman's equation. In general, the solution for the Boltzman's equation is very difficult unless for some limiting cases. These limiting cases can be identified with the help of Knudsen number. The Knudsen number is defined as the ratio of the gas mean free path  $l$  to a characteristic length scale of the particle,  $Kn = l/a$ . The characteristic length scale is assumed to be the equivalent-volume radius  $a$  of the particle.

### 2.2.3 Knudsen Number

The Knudsen number can be classified into three regimes: the continuum regime ( $Kn \ll 1$ ), the transition regime ( $Kn \sim 1$ ), and the free-molecule regime ( $Kn \gg 1$ ). The Boltzmann equation is an integro-differential equation and solution of this equation is limited to few cases. The continuum based models are the Navier-Stokes equations. Euler equations correspond to inviscid continuum limit which shows a singular limit since the fluid is assumed to be inviscid and non-conducting. Euler flow corresponds to  $Kn = 0$ . The Navier-Stokes equations can be derived from the Boltzmann equation using the Chapman-Enskog expansion. At Knudsen numbers larger than 0.1 the Navier-Stokes equations break-down and a higher level of approximation is obtained by carrying second order terms (in  $Kn$ ) in the Chapman-Enskog

expansion. A special form of such an equation is called the Burnett equation, for which the solution requires second-order accurate slip boundary conditions in  $Kn$ . The Burnett equations and consistent second-order slip boundary conditions is subject to some controversy and a better way of solving high Knudsen number flow is through molecular based direct simulation techniques such as the Direct Simulation Monte Carlo method (DSMC) [8].

### **Continuum Regime**

The thermophoresis theory in continuum regime ( $Kn \ll 1$ ) can be built upon the solution of the Navier-Stokes equations combined with the appropriate slip boundary conditions. The boundary conditions are based on the temperature jump and thermal creep. This accounts for the fact that the gas cannot be treated as a continuous medium within a few mean free paths from the particle surface [8].

### **Transition Regime**

In this range of Knudsen number ( $Kn \sim 1$ ), the theoretical solutions are the most difficult to obtain [8]. However, interpolation models were advocated by researchers [9, 10] for finding results in transition regime. Brock's near-continuum solution was a widely used formula for interpolation until more accurate solutions to Boltzmann's equation became available [11]. In the limit  $Kn \rightarrow \infty$ , Brock's near continuum solution got reduced to a form very similar (differs only by a constant) to the free molecular solution of Waldmann. Therefore, this formula was used for obtaining results in the transition regime.

## Free-molecular Regime

In the limit of  $Kn \gg 1$  the velocity distribution function of the incoming molecules is not affected by the presence of the particle. To calculate the thermophoretic force, it is necessary to model the behavior in which the gas molecules are reflected by the particle surface after collisions with the particle [8].

With the literature presented in the above sections, we can begin with the proposed methodology. Chapter 3 will present details of the proposed methodology and the algorithm employed. The chapter will be divided broadly into two major sections: (1) two-particle model, and (2) aggregate model.

## CHAPTER 3

### THE MODEL

#### 3.1 The velocity distribution function

The molecules in a gas possess a velocity distribution function, which characterizes the speed and direction of molecular travel. Typically the distribution is a function of 6 coordinates: 3 spatial coordinates ( $x, y, z$ ) and three velocity coordinates ( $u, v, w$ ). Together, these 6 coordinates are referred to as phase space.

We can assume for now that the properties of the gas are uniform over space, so that the distribution function only depends on the three velocity components. For this case, the distribution, denoted as  $f$ , is defined so that

$$f(u, v, w) du dv dw$$

is the number of molecules per unit volume that have velocities within  $du$  of  $u$ ,  $dv$  of  $v$ , and  $dw$  of  $w$ . In addition,

$$n = \int_{-\infty}^{\infty} du \int_{-\infty}^{\infty} dv \int_{-\infty}^{\infty} dw f(u, v, w) \quad (3.1)$$

in which  $n$  is the number density (number of molecules per unit volume, units of  $1/\text{m}^3$ ). This shows that the distribution function must have units of number density/velocity<sup>3</sup>, or  $\text{s}/\text{m}^6$ . For an equilibrium gas (stationary and at a uniform temperature), the distribution is given by the Maxwellian formula:

$$f = \frac{n}{\pi^{3/2} C_T^3} \exp [-(u^2 + v^2 + w^2)/C_T^2] \quad (3.2)$$

in which  $C_T = \sqrt{2RT}$  is the thermal speed of the molecules, with  $R$  being the specific gas constant.

A polar coordinate system is often used to characterize the molecular velocity, with

$$du dv dw = c^2 dc \sin\theta d\theta d\phi$$

in which  $c$  is the molecular speed,

$$c^2 = u^2 + v^2 + w^2$$

and  $\theta$  and  $\phi$  are the polar and azimuthal angles of the molecular trajectory;

$$u = c \sin\theta \cos\phi$$

$$v = c \sin\theta \sin\phi$$

$$w = c \cos\theta$$

Averages (or moments) of the distribution function are obtained via

$$\langle \psi \rangle = \frac{1}{n} \int_{c=0}^{\infty} \int_{\theta=0}^{\pi} \int_{\phi=0}^{2\pi} \psi f c^2 dc \sin\theta d\theta d\phi \quad (3.3)$$

in which  $\psi$  is some molecular quantity. For example, the average speed is obtained by setting  $\psi = c$ . For the maxwellian distribution, this gives

$$\langle c \rangle = \frac{2}{\sqrt{\pi}} C_T = \sqrt{\frac{8RT}{\pi}}$$

and the mean kinetic energy, per unit mass, is obtained from setting  $\psi = c^2/2$ , or

$$\langle c \rangle = \frac{3}{4} C_T^2 = \frac{3}{2} RT$$



The *flux* of a molecular quantity  $\psi$  refers to the transport of  $\psi$  across a surface (real or imaginary) in the direction normal to the surface and per unit area of the surface. It would have unit of  $\psi$  /m<sup>2</sup>/s. Say that the normal to the surface points in the  $z$  direction. The formula for the flux is obtained from

$$j_\psi = \int_{u=-\infty}^{\infty} \int_{v=-\infty}^{\infty} \int_{w=0}^{\infty} \psi f w \, du \, dv \, dw \quad (3.4)$$

or, in polar coordinates,

$$j_\psi = \int_{c=0}^{\infty} \int_{\theta=0}^{\pi/2} \int_{\phi=0}^{2\pi} \psi f c \cos\theta \, c^2 \, dc \, \sin\theta \, d\theta \, d\phi \quad (3.5)$$

The number flux is obtained by setting  $\psi = 1$ , and for the maxwellian distribution,

$$j_n = \frac{1}{2\sqrt{\pi}} n C_T$$

The momentum flux in the  $z$  direction is obtained from  $\psi = mw = mc \cos\theta$  (with  $m$  the molecule mass), and

$$j_{mom} = \frac{1}{4} mn C_T^2 = \frac{1}{2} \rho RT$$

in which  $\rho = mn$  is the mass density. From the ideal gas law the momentum flux is equal to  $P/2$  which represents the normal stress on the (imaginary) surface due to molecules leaving the surface. If we calculated the flux of momentum arriving at the surface we would also get  $P/2$ , and the total stress would be  $P$ , as expected.

The net force acting on an object (a particle, for example) would be obtained by integrating the net momentum flux (incident and reflected) over the surface of the particle.

### 3.2 Sampling of the distribution function

In our work we assume, beforehand, that we know the distribution function(s) of the molecules incident on the particles (targets) and emitted from the particles (i.e., reflected). From this, we can compute the transfer of quantities (momentum, energy) to and from the targets. However, the targets will possess a geometry which would make difficult an analytical evaluation of the integrals per the previous formulas. Consequently, we will numerically compute the transport of momentum and energy via a monte carlo method.

The MC method is conceptually straightforward. We simulate molecular trajectories and observe (on a computer) how the molecules interact with the target. By collecting averages over the simulation of a large number of molecules, we can determine the net rate of momentum and energy transfer to the target.

A required element to implementing the MC method is the sampling of a distribution function. For example, we may know that the molecules which we are simulating have a velocity that is described by a given velocity distribution function. We want to *randomly* assign values of velocity to individual molecules so that, when averaged over a large number of molecules, the velocities fall into a distribution that is consistent with our modelled distribution.

The sampling approach that we follow for this thesis would be cumulative distribution approach. Say our distribution is a function of one variable,  $x$ , and that  $x$  runs from 0 to 1 ( $x$  is arbitrary here; it does not have a physical interpretation). The

cumulative distribution function, denoted  $g(x)$ , is defined by

$$g(x) = \frac{\int_0^x f(t) dt}{\int_0^1 f(t) dt}$$

in which  $t$  is a dummy variable of integration. The cumulative distribution  $g(x)$  represents the probability of choosing a sample from  $f$  that is between 0 and  $x$ . If  $x = 1$  then  $g = 1$ , i.e., we are certain that  $x$  lies between 0 and 1. On the other hand, if we set  $g = 1/2$  we would get an equation for  $x_m$  (referred to as the mode of the distribution):

$$1/2 = g(x_m) \rightarrow x_m = g^{-1}(1/2)$$

in which  $g^{-1}$  is the inverse of the cumulative distribution function. The interpretation of  $x_m$  is that it is equally likely (50/50 chance) that a sampled  $x$  will lie either above or below  $x_m$ . This does not imply that  $x_m = 1/2$ ; the value of  $x_m$  depends on the form of the distribution function.

To construct a sampling scheme, we first note that all values of  $g$  are equally likely. That is, from a probabilistic point of view,  $g$  will be uniformly distributed between 0 and 1. We can then set  $g$  equal to a uniform random number between 0 and 1 to obtain

$$g(x) = \mathbf{R}$$

in which  $\mathbf{R}$  is the random number between 0 and 1. The sampled  $x$  is obtained from the inverse function;

$$x = g^{-1}(\mathbf{R})$$

### 3.3 The two sphere model

A basic starting model for our analysis is as follows. A pair of identical spheres of radii  $a$  are separated by a distance  $R$ . The spheres are contained in a gas, and the mean free path of the gas molecules is significantly larger than the largest geometrical length. The gas is at temperature  $T_0$  and pressure  $P_0$ . The spheres are at a uniform temperature  $T_S < T_0$ ; this temperature difference is maintained by radiation heat emission from the spheres. We wish to calculate the following:

1. The rate of radiation heat transfer necessary to maintain the given temperature difference  $T_0 - T_S$ . In principle, we would know the heat transfer rate from an analysis of radiation and from this we would calculate  $T_S$ . However, the problem will be somewhat simplified if we assume that  $T_S$  is given.
2. The net force acting between the two spheres as a result of differences in the molecular momentum flux on the sphere surfaces.

Assumptions we will make are

1. The spheres are stationary: they are held in place by some invisible means. This is a contrived problem, but we need to start somewhere.
2. The gas is stationary: no bulk motion.
3. The surfaces of the spheres have perfect momentum and energy accommodation. All previous history of the molecular trajectory is lost upon collision with the surface. Re-emission of the molecules is diffuse.

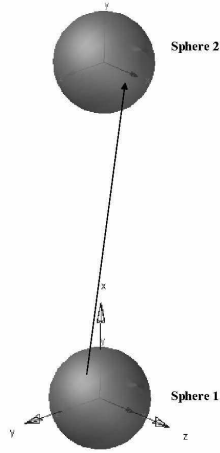


Figure 3.1: Two–sphere model showing the ray trace of a molecule

4. Free molecular limit conditions:  $Kn \gg 1$ . There are no molecule-molecule collisions. The soot particles we consider would be nearly nano-sized, making them considerably smaller than the mean free path. This assumption is supported by the gas temperatures we would be dealing with ( $\sim 1500\text{ K}$ ). At such high temperatures, the mean free path increases, thus justifying our assumption of  $Kn \gg 1$  (i.e., the mean free path  $\gg$  the particle size). Typically, the soot particles are  $0.01\ \mu\text{m}$  in size, whereas the mean free path at STP is of the order  $0.065\ \mu\text{m}$ . At around a temperature of  $2000\text{ K}$ , it is of the order of  $0.3\ \mu\text{m}$ .
5. The incoming molecules from the background gas are characterized by a maxwellian velocity distribution at temperature  $T_0$  and number density  $n_0$ .
6. The re-emitted molecules (i.e., reflected molecules) are characterized by a maxwellian distribution at  $T_S$  and number density  $n_S$ .

### 3.3.1 Energy transport

Label the spheres 1 and 2 (because of the symmetry of the problem, conditions/transfer rates will be identical for both spheres, but we will distinguish between the spheres anyway). The net rate of molecular kinetic energy transfer to sphere 1, due to molecular collisions, is

$$\dot{Q}_{m,1} = \int_A \int_{\Omega} \int_{c=0}^{\infty} (f_{in} - f_S) \frac{1}{2} m c^2 \hat{\mathbf{n}} \cdot \mathbf{c} c^2 dc d\Omega dA \quad (3.6)$$

in which  $m$  is the molecular mass,  $\hat{\mathbf{n}}$  the outward normal,  $\mathbf{c}$  the molecular velocity vector,  $A$  the surface area of the sphere, and  $d\Omega = \sin\theta d\theta d\phi$  is a differential solid angle. The velocity distribution functions  $f_{in}$  and  $f_S$  describe the incoming and emitted (reflected) molecules, respectively.

The integrals in 3.6 cannot be trivially performed analytically because  $f_{in}$  will be a function of incoming direction and surface position. For positions on the hemisphere facing the opposite sphere, part of the incoming molecules will originate from the opposite sphere, and the remainder will originate from the background gas.

When the incoming direction points towards the opposite sphere the incoming distribution will be  $f_{in} = f_S$ ; this is because we assume that the temperatures of both spheres are identical. Consequently, the integrand in 3.6 will vanish for directions  $\Omega$  pointed towards the opposite sphere. For direction pointed towards the background gas we will have  $f_{in} = f_0$ , and 3.6 becomes

$$\dot{Q}_{m,1} = \int_A \int_{\Omega_0} \int_{c=0}^{\infty} (f_0 - f_S) \frac{1}{2} m c^2 \hat{\mathbf{n}} \cdot \mathbf{c} c^2 dc d\Omega dA \quad (3.7)$$

in which  $\Omega_0$  denotes the directions which point towards the background gas; this will be a function of position on the sphere.

The distribution functions are given by

$$f_S = \frac{n_S}{\pi^{3/2} C_{T,S}^3} \exp(-c^2/C_{T,S}^2) \quad (3.8)$$

$$f_0 = \frac{n_0}{\pi^{3/2} C_{T,0}^3} \exp(-c^2/C_{T,0}^2) \quad (3.9)$$

with  $C_{T,S} = \sqrt{2RT_S}$  and likewise for  $C_{T,0}$ .

The integral over speed  $c$  can be performed analytically in 3.7, and the remaining integrals over direction and position will define a configuration factor  $F_{1-0}$  so that

$$\dot{Q}_{m,1} = \frac{m}{2\pi^{1/2}} (n_0 C_{T,0}^3 - n_S C_{T,S}^3) 4\pi a^2 F_{1-0} \quad (3.10)$$

in which

$$4\pi a^2 F_{1-0} = \frac{1}{\pi} \int_A \int_{\Omega_0} \hat{\mathbf{n}} \cdot \mathbf{s} \, d\Omega \, dA \quad (3.11)$$

with  $s$  being a unit vector which points in all directions except towards the opposite sphere. The quantity  $F_{1-0}$  is identical to the radiation configuration factor which is used in radiation exchange problems; it represents the fraction of all emitted molecules from 1 which travel to the background gas. By summation we have  $F_{1-0} + F_{1-2} = 1$ , i.e., the emitted molecules either end up in the background gas or on sphere 2.  $F_{1-0}$  is a function only of the distance between the centers of the two spheres.

Equation 3.10 contains the unknown quantity  $n_S$ , which can be determined by application of mass transfer principles. The net molecular flux at any point on the surface must be zero, i.e., the incoming flux must balance the outgoing flux. This leads to

$$J_n = 0 = \int_{\Omega} \int_{c=0}^{\infty} (f_S - f_{in}) \hat{\mathbf{n}} \cdot \mathbf{c} c^2 dc d\Omega \quad (3.12)$$

Again, the incoming distribution depends on the position on the sphere. As before, the integral over direction  $\Omega$  can be split into a fraction  $\Omega_S$  which includes all directions which point to the neighboring sphere, and  $\Omega_0$  which encompasses all directions which point towards the background gas. For the former case the incoming distribution function will be  $f_S$  and for the latter the distribution will be  $f_0$ . The integral is then

$$J_n = 0 = \int_{\Omega_0} \int_{c=0}^{\infty} (f_S - f_0) \hat{\mathbf{n}} \cdot \mathbf{c} c^2 dc d\Omega \quad (3.13)$$

Since this result must hold at every point on the surface - and since  $\Omega_0$  is a function of surface position - it follows that

$$\int_{c=0}^{\infty} (f_S - f_0) c c^2 dc = 0 \quad (3.14)$$

The integrals can be computed analytically, which gives

$$n_S C_{T,S} = n_0 C_{T,0} \quad (3.15)$$

which provides a relation between the number densities and temperatures of the incoming and emitted molecules.



By putting the above into 3.10, we get

$$\dot{Q}_{m,1} = \frac{\rho_0 C_{T,0}}{2\pi^{1/2}} (C_{T,0}^2 - C_{T,S}^2) 4\pi a^2 F_{1-0} \quad (3.16)$$

$$= \frac{\rho_0 R C_{T,0}}{\pi^{1/2}} (T_0 - T_S) 4\pi a^2 F_{1-0} \quad (3.17)$$

### 3.3.2 Momentum transfer

The force applied to the sphere due to the emitted molecules will be zero, due to the fact that the emitted molecules are emitted isotropically (uniform in all directions). The net force is therefore due to the nonuniformity in the incoming molecules, and will be given by

$$\mathbf{F}_1 = \int_A \int_{\Omega} \int_{c=0}^{\infty} f_{in} m \mathbf{c} (\hat{\mathbf{n}} \cdot \mathbf{c}) c^2 dc d\Omega dA \quad (3.18)$$

As before, the integral over direction  $\Omega$  can be split into  $\Omega_S$  and  $\Omega_0$  and  $f_{in}$  will have the corresponding value of  $f_S$  or  $f_0$ . We can then use

$$\begin{aligned} \int_A \int_{\Omega_0} \int_{c=0}^{\infty} f_0 m \mathbf{c} (\hat{\mathbf{n}} \cdot \mathbf{c}) c^2 dc d\Omega dA &= \left( \int_A \int_{\Omega} \int_{c=0}^{\infty} f_0 m \mathbf{c} (\hat{\mathbf{n}} \cdot \mathbf{c}) c^2 dc d\Omega dA \right. \\ &\quad \left. - \int_A \int_{\Omega_S} \int_{c=0}^{\infty} f_0 m \mathbf{c} (\hat{\mathbf{n}} \cdot \mathbf{c}) c^2 dc d\Omega dA \right) \\ &= - \int_A \int_{\Omega_S} \int_{c=0}^{\infty} f_0 m \mathbf{c} (\hat{\mathbf{n}} \cdot \mathbf{c}) c^2 dc d\Omega dA \end{aligned}$$

The integral over all directions  $\Omega$  in the above is zero because the momentum flux for this part is isotropic. We then get

$$\mathbf{F}_1 = \int_A \int_{\Omega_S} \int_{c=0}^{\infty} (f_S - f_0) m \mathbf{c} (\hat{\mathbf{n}} \cdot \mathbf{c}) c^2 dc d\Omega dA \quad (3.19)$$

with the integral over direction limited to directions which point from 1 to 2.

The integrals over speed can be performed analytically, to give

$$\mathbf{F}_1 = \frac{3m}{8\pi} (n_S C_{T,S}^2 - n_0 C_{T,0}^2) 4\pi a^2 \mathbf{G}_{1-2} \quad (3.20)$$

in which  $\mathbf{G}_{1-2}$  is a vector which depends only on the geometry. For a pair of spheres, components will be aligned with axis of symmetry.

$$4\pi a^2 \mathbf{G}_{1-2} = \frac{1}{\pi} \int_A \int_{\Omega_S} \mathbf{s} (\hat{\mathbf{n}} \cdot \mathbf{s}) d\Omega dA \quad (3.21)$$

Using 3.15 in 3.20 gives

$$\mathbf{F}_1 = \frac{3\rho C_{T,0}}{8\pi} (C_{T,S} - C_{T,0}) 4\pi a^2 \mathbf{G}_{1-2} \quad (3.22)$$

### 3.3.3 Soot radiation heat source function

This section presents a simplified derivation of the rate of thermal emission from a carbonaceous soot particle. The derivation begins with correlations from [12] on the absorption properties of a soot cloud, and backs out the rate at which a single particle will emit radiation.

The rate of emission from a particle cloud, per unit volume of the cloud, will be

$$q_e''' = 4 \kappa_p e_b, \quad W/m^3 \quad (3.23)$$

where  $\kappa_p$  is the Planck mean absorption coefficient, defined by

$$\kappa_p = \int_0^\infty \kappa_\lambda e_{b\lambda} d\lambda \quad (3.24)$$

where  $\lambda$  is wavelength and

$$e_{b\lambda} = \frac{C_1}{\lambda^5 (\exp(C_2/\lambda T) - 1)}, \quad e_b = \int_0^\infty e_{b\lambda} d\lambda = \sigma T^4$$

where  $\sigma = 5.67 \times 10^{-8} W/(m^2.K^4)$ , are the spectral and total blackbody emissive power functions.

The spectral absorption coefficient  $\kappa_\lambda$  for carbon soot can be approximated as

$$\kappa_\lambda \approx \frac{7f}{\lambda}, \quad \mu m^{-1}$$

where  $f$  is the soot volume fraction (volume of the solid particle per unit volume of medium; a dimensionless quantity). Replacing this into 3.24 and integrating gives

$$\kappa_p = 1.86 \times 10^3 f T, \quad m^{-1}$$

Using the above formulas, the emissive sink for the soot cloud will be

$$q_e''' = 4 \kappa_p e_b = C_k f T^5$$

where  $C_k = 4.23 \times 10^{-4} \text{ W/m}^3\text{K}^5$ .

Assuming all particles are identical, the rate of emission per unit cloud volume would be related to the cloud number density by

$$q_e''' = Q_e n$$

in which  $n$  is the number density of the particles and  $Q_e$  is the rate of emission from a single particle. Likewise, the volume fraction of the cloud would be given by

$$f = V n$$

with  $V$  being the particle volume. Using these relations results in

$$Q_e = C_k V T^5$$

with  $V$  given in  $m^3$ . If we assume that the particles are spherical with radius  $a$ , we get

$$Q_e = \frac{4\pi}{3} C_k a^3 T^5 \tag{3.25}$$

From 3.16 the rate of molecular energy transfer to the particle was

$$\dot{Q}_{m,1} = \frac{\rho_0 C_{T,0}}{2\pi^{1/2}} (C_{T,0}^2 - C_{T,S}^2) 4\pi a^2 F_{1-0} \quad (3.26)$$

$$\approx \frac{\rho_0 C_{T,0}^2}{\pi^{1/2}} (C_{T,0} - C_{T,S}) 4\pi a^2 F_{1-0} \quad (3.27)$$

the last line using a first order approximation for small  $C_{T,0} - C_{T,S}$ . It should be noted here that the rationale for assuming  $C_{T,0} - C_{T,S}$  is that  $T_S$  has a value of around 1499.54  $K$  when  $T_0 = 1500 K$  at  $a = 15nm$ . Hence the perturbation on the spheres can be assumed to be negligible. By setting  $Q_{m,1} = -Q_e$ , we get

$$C_{T,S} - C_{T,0} = \frac{\sqrt{\pi} Q_e}{\rho_0 C_{T,0}^2 4\pi a^2 F_{1-0}} \quad (3.28)$$

The force acting between a pair of spheres was

$$\mathbf{F}_1 = \frac{3\rho C_{T,0}}{8\pi} (C_{T,S} - C_{T,0}) 4\pi a^2 \mathbf{G}_{1-2}$$

or, using the previous equation, 3.28,

$$\mathbf{F}_1 = \frac{3Q_e}{8\sqrt{\pi} C_{T,0}} \frac{\mathbf{G}_{1-2}}{F_{1-0}} \quad (3.29)$$

Using the formula for  $Q_e$ , 3.25, the above result shows that 1) the force will scale with  $a^3$  (i.e., proportional to the particle volume), and 2) the force will scale with  $T_0^{4.5}$ , and  $\mathbf{G}_{1-2}$  will scale (asymptotically) as  $(a/r_{1-2})^2$ .

### 3.3.4 Thermophoretic force analysis

The thermophoretic force analysis can be borrowed from thoroughly-investigated phenomenon of coagulation between *electrically charged* particles [12] as discussed by [13]. The force existing between the electrically charged particles follows an inverse-square law and is an instantaneous force. However, the case of effective thermophoretic force is not precisely equivalent to the instantaneous force in electrostatics [13]. This is because the interaction of the thermophoretic force takes place through the carrier gas and an inverse-square relationship would hold good only when the characteristic time of gas heat transfer propagation is considerably smaller than the characteristic time of the particle motion [13]. In the present analysis, however, an inverse-square relationship can be approximated taking into account that we are dealing with  $\mu m$ - sized particles, the ratio of gas to particle characteristic times for which is of the order of 0.1 - good enough for the above mentioned approximation [13].

From the electrical analogy, the ratio of coagulation rate constants between the two particles with thermophoresis to that due to Brownian motion alone, is expressed [12] as

$$Z = \frac{y}{e^y - 1}$$

where

$$y = \frac{F_{12} r_{12}}{K_B T_g}$$

where  $r_{12}$  is the separation distance at contact,  $K_B = 1.3805 \times 10^{-23} \text{ J/K}$  is Boltzmann's constant,  $T_g$  is the temperature of the gas, and  $F_{12}$  is the force at contact

between the spheres given [12] by

$$F_{12} = \nu\mu \frac{e^2}{r_{12}^2} \quad (3.30)$$

where  $\nu$  and  $\mu$  are the number of the elementary electrical charges (electron charges),  $e$ . In the above equation

Comparing 3.29 and 3.30, i.e., replacing electrostatic force ( $F_{12}$ ) with thermophoretic force ( $\mathbf{F}_1$ ), we have for  $y$ :

$$y = 2 \times \frac{3Q_e}{8\sqrt{\pi}C_{T,0}} \frac{\mathbf{G}_{1-2}}{F_{1-0}} \frac{r_{12}}{K_B T_g} \quad (3.31)$$

with  $\mathbf{G}_{1-2}$  and  $\mathbf{F}_{1-0}$  evaluated at contact, i.e., at  $r_{12} = 2a$ . Using the expression for  $Q_e$  from 3.25 in 3.31 and 3.29 and substituting the values of all constants, we get

$$y = -(4.5212 \times 10^{18}) a^4 T_g^{3.5} \left( \frac{\mathbf{G}_{1-2}}{F_{1-0}} \right) \quad (3.32)$$

and

$$\mathbf{F}_T = 2 \times \mathbf{F}_1 = (3.1208 \times 10^{-5}) a^3 T_g^{4.5} \left( \frac{\mathbf{G}_{1-2}}{F_{1-0}} \right) \quad (3.33)$$

respectively.  $\mathbf{F}_1$  is multiplied by a factor 2 to get  $\mathbf{F}_T$  because  $\mathbf{F}_1$  is the force acting on a single sphere and  $\mathbf{F}_T$  is the total thermophoretic force between the two spheres. The units of  $a$  and  $\mathbf{F}_T$  in the above equation are  $m$  and  $N$  respectively.

### 3.3.5 Monte Carlo method

The computational study of this thesis is done in MATLAB 6.5 version. The basic outline of the algorithm we are going to implement using a monte carlo technique is

1. to release *computational gas molecules* from *random* points on the surface of sphere 1 in *random* directions
2. track the molecule, determine where it ends up
3. repeat the code several times
4. compute  $F_{1-0}$  and  $\mathbf{G}_{1-2}$  and
5. hence compute  $y$  and  $\mathbf{F}_T$ .

#### Sampling the position on sphere surface

To start with the monte carlo technique, we first sample the position on the surface of sphere 1 from which molecules are released. The pseudo-random number generator of MATLAB is used for all random sampling purposes in this thesis.

The polar and azimuth angles of the position on the surface are sampled from the cumulative distribution functions represented by

$$\mathbf{R}_1 = \int_0^{\cos\theta} d(\cos\theta)$$

$$\mathbf{R}_2 = \frac{1}{2\pi} \int_0^\phi d\phi$$



where  $\mathbf{R}$  is the random number generator between 0 and 1. Upon inversion, we have

$$\cos\theta_1 = \mathbf{R}_1 \quad (3.34)$$

$$\phi_1 = 2\pi\mathbf{R}_2 \quad (3.35)$$

We have sampled  $\cos\theta_1$  from 0 to 1, and not -1 to 1 because, the molecules released from the hemisphere of sphere 1 not facing the second sphere do not end up on it anyway.

### Sampling the direction of molecules

The polar and azimuth angles of the direction of the molecule released from the sphere surface are represented by

$$\mathbf{R}_3 = 2 \int_0^{\cos\theta} \cos\theta \, d(\cos\theta)$$

$$\mathbf{R}_4 = \frac{1}{2\pi} \int_0^\phi d\phi$$

Upon inversion, we have

$$\cos\theta_2 = \sqrt{\mathbf{R}_3} \quad (3.36)$$

$$\phi_2 = 2\pi\mathbf{R}_4 \quad (3.37)$$

## Determination of collision point

The method followed to determine the collision point (or, for that matter, if the molecule collides with the sphere 2 or not) by [14] is employed here.

The distance of the molecule starting point  $(x_0, y_0, z_0)$  to the center of sphere 2  $(x_s, y_s, z_s)$  is

$$r_{s0} = ((x_s - x_0)^2 + (y_s - y_0)^2 + (z_s - z_0)^2)^{1/2} \quad (3.38)$$

If  $r_{ms}$  is the distance between the molecule, at any point in its trajectory, and the center of sphere 2, then the minimum value of  $r_{ms}$  will occur when  $\mathbf{r}_{ms} \cdot \hat{\mathbf{c}} = 0$  [14].

$$\Rightarrow r_{ms} = r_{s0} \sin \alpha \quad (3.39)$$

where  $\alpha$  is the angle between the molecular trajectory and the position vector of the center of sphere 2 relative to the starting point, i.e.,

$$\cos \alpha = \frac{1}{r_{s0}} [(x_s - x_0) \hat{u} + (y_s - y_0) \hat{v} + (z_s - z_0) \hat{w}] \quad (3.40)$$

where  $(\hat{u}, \hat{v}, \hat{w})$ , the trajectory of the molecule is given by [14]

$$\hat{u} = \cos \phi_1 (\sin \theta_2 \cos \phi_2 \cos \theta_1 + \cos \theta_2 \sin \theta_1) - \sin \phi_1 \sin \theta_2 \sin \phi_2 \quad (3.41)$$

$$\hat{v} = \sin \phi_1 (\sin \theta_2 \cos \phi_2 \cos \theta_1 + \cos \theta_2 \sin \theta_1) - \cos \phi_1 \sin \theta_2 \sin \phi_2 \quad (3.42)$$

$$\hat{w} = \cos \theta_2 \cos \theta_1 - \sin \theta_2 \cos \phi_2 \sin \theta_1 \quad (3.43)$$

If  $r_{ms} \leq a$ , then the molecule has collided with the sphere 2 [14].

The molecules are released one-by-one and the above process is repeated several number of times. Finally, the configuration factor,  $F_{1-2}$ , is obtained by dividing the number of molecules that collided with the sphere 2 by the total number of molecules released. The subsequent calculations of  $y$  and  $\mathbf{F}_T$  are carried out by using equations 3.32 and 3.33.

### 3.4 Aggregate model

In this case, we consider the interaction between a sphere and a cluster of spheres (of identical radii). The cluster is synthesized based on the power-law, 2.1. The algorithm used for this synthesis is the one used in [14]. The program is run and a cluster of 25 spheres is generated.

Sampling of the distribution function for the aggregate model is the same as that done for the two-sphere model. The equations for energy transport, momentum transfer, the soot radiation heat source function, and the thermophoretic force analysis remain the same with the two-sphere model directly extended to multiple sphere, i.e., with  $\mathbf{G}_{1-2} \longrightarrow \mathbf{G}_{1-i}$ .

The only modification for the aggregate model would appear in the monte carlo code written for the two-sphere model.

#### 3.4.1 Modified Monte Carlo method

The algorithm of the modified monte carlo technique would be

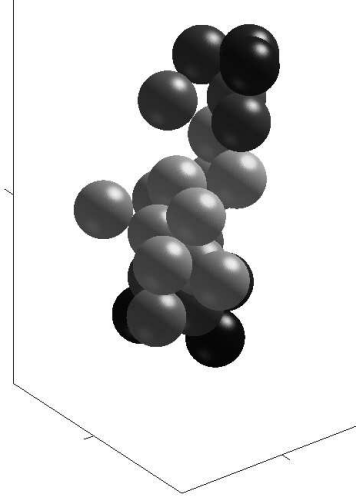


Figure 3.2: Soot aggregate generated using the power law

1. release of *computational gas molecules* from *random* points on the surface of sphere 1 in *random* directions
2. track the molecule, determine if it ends up on the cluster
3. calculate the overall configuration factor,  $\mathbf{F}_{1-cluster}$  by repeating the code several times. The overall configuration factor is calculated as  $\mathbf{F}_{1-cluster} = \sum_{i=1}^N \mathbf{F}_{1-i}$ .
4. compute  $\mathbf{G}_{1-cluster}$  and
5. hence compute  $y_{cluster}$  and  $\mathbf{F}_{T_{cluster}}$ .

Sampling the position on sphere surface and sampling the direction of molecules are done in the same fashion as that for the two-sphere model. The determination of the collision point (figure 3.3) on the cluster is also done in a more advanced

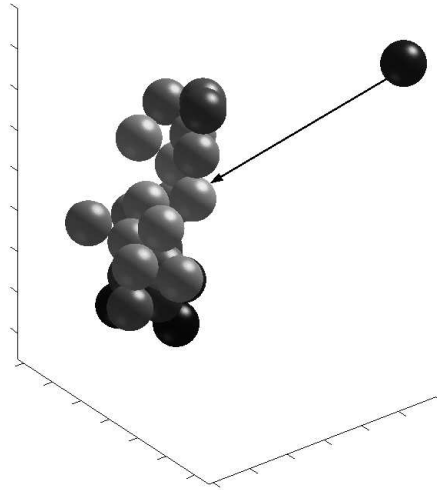


Figure 3.3: Aggregate–model showing the ray trace of a molecule

fashion, noting the complex geometry that is involved in this case. The procedure is as follows: When a molecule is released from sphere 1, its trajectory is followed and the perpendicular distances from the individual spheres in the cluster to this trajectory are determined. All the distances that are less than the sphere radius,  $a$  are noted. Now, using the law of cosines the distance the molecule has travelled at the collision point,  $s_c$  is determined for all spheres that met the above condition. Among the obtained values the one which has the minimum  $s_c$  is identified to be the sphere with which the molecule has collided.

## CHAPTER 4

### RESULTS AND CONCLUSIONS

#### 4.1 Results

The monte carlo code for both the two–sphere model and the aggregate model was written in MatLab 6.5. The program was run on a PC with Intel Pentium 4 processor, 1.4 GHz and 512 MB of RAM.

##### 4.1.1 The two sphere model

The two spheres under consideration had the same radius ( $= 0.01 \mu m$ ). The temperature of the gas was taken to be 1500 K. The monte carlo code for the two–sphere model comprised of release of 250,000 computational molecules from sphere 1. The program took around 4 minutes to give the output, i.e., the force between the spheres, the coagulation ratio, and the plot between the force and the distance between the two spheres.

Plotted in fig. 4.1 is the thermophoretic force, in  $N$ , between the two spheres versus the distance, in  $m$ , between them. As it can be seen from the figure, the force between the two spheres follows an inverse–squared variation with the distance.

The plot in fig. 4.2 represents the plot shown in fig. 4.1 on a log–log scale. The plot has a slope of  $-2$ . The distortion of the plot towards the larger values of distance is the ‘noise’. This should be expected because for higher values of distance between the spheres, the configuration factor,  $\mathbf{F}_{1-2}$ , identically approaches zero and the monte carlo technique in such a case would fail.

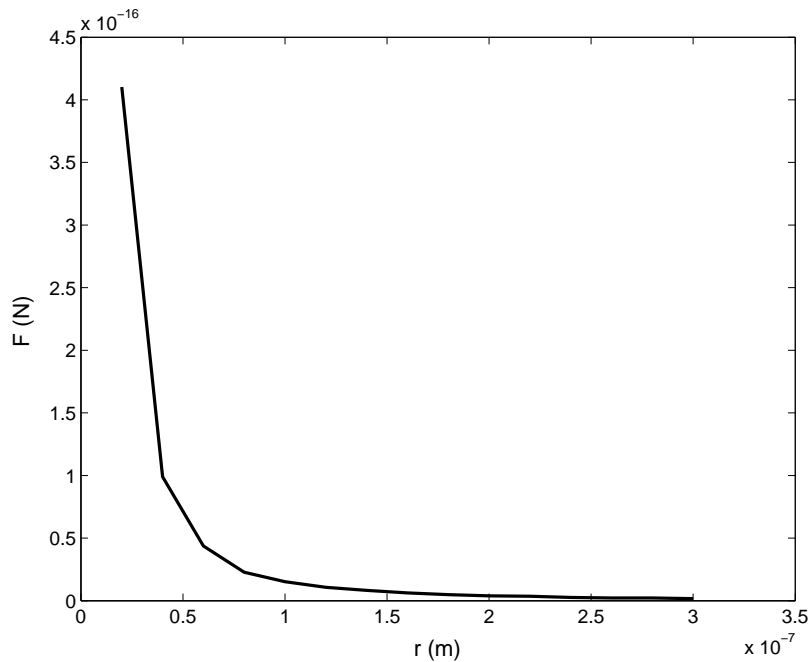


Figure 4.1: Two sphere model – Force vs Distance

The coagulation ratio,  $Z$ , for this model was observed to be around 1.0002, for a sphere radius of  $0.01 \mu m$  and a gas temperature of  $1500 K$ .

#### 4.1.2 Aggregate model

The main task here would be to decide on the number of computational molecules to be released from sphere 1 on to the cluster. For this, we first collect samples comprising of, say, 100 molecules. The configuration factor from sphere 1 to the cluster ( $F_{1-cluster}$ ) is determined for each such sample. Every time, a group of 10 such samples is taken and the ratio of standard deviation to the mean of that group is calculated. The first group would consist of samples 1 through 10, the next one consists of samples 2 through 11, and so on. The algorithm is written in such a

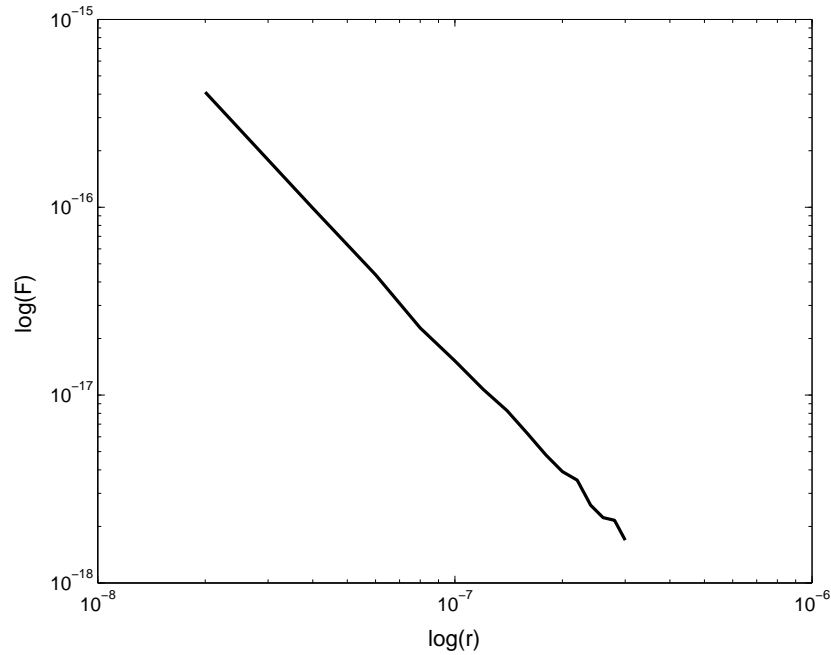


Figure 4.2: Log–Log scale of Fig.4.1

way that the release of molecules will be terminated when the above mentioned ratio becomes less than or equal to 0.0005. This means that we are allowing 99.95% of accuracy.

Fig. 4.3 shows the plot of the configuration factor,  $F_{1-cluster}$  versus the number of samples of the computational molecules,  $N_{samp}$ , released. In the monte carlo code, we have set the total number of molecules to be released as 100000, but the computation stops when the total number of molecules reach a value of around 53000 because the desired accuracy level is reached by this number, thus saving the computation time.

A cluster consisting of 25 spheres was generated, all with same radii as that of the sphere 1 ( $= 0.01 \mu m$ ). The temperature of the gas was taken to be 1500 K. The accuracy for ( $F_{1-cluster}$ ) was set to 99.9% and 100,000 computational molecules from



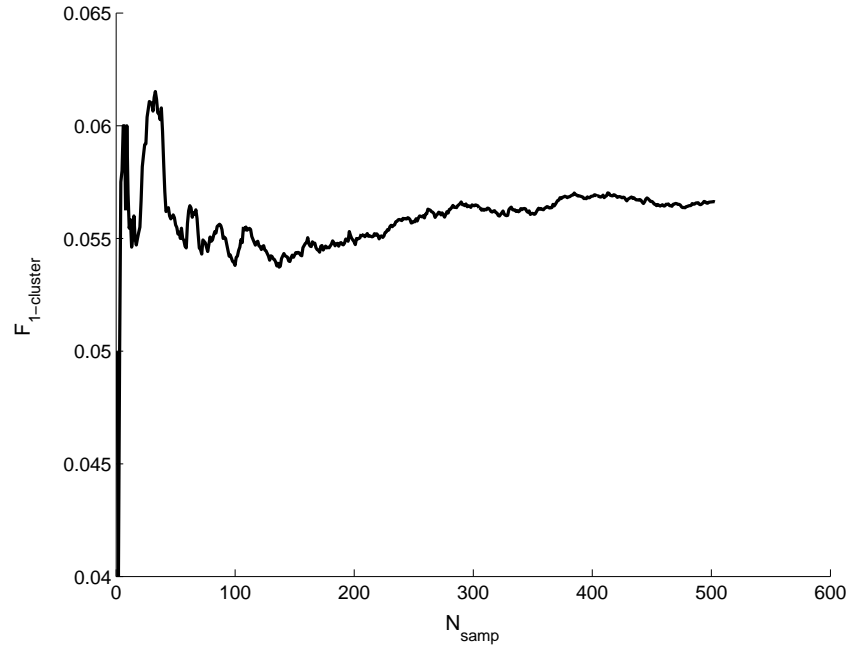


Figure 4.3:  $F_{1-cluster}$  vs  $N_{samp}$

sphere 1 were released. The position of sphere 1 relative to the cluster is randomly chosen around the cluster. The program took around 25 minutes to give the output, i.e., the force between the spheres, the coagulation ratio, and the plot between the force and the distance between the two spheres.

Fig. 4.4 shows the variation of the thermophoretic force in  $N$  between sphere 1 and the cluster with the distance in  $m$  between sphere 1 and the center of mass of the cluster. As was the case with the two sphere model, the force in the aggregate model bears an inverse-squared relationship with the distance. The magnitudes of the force in the two cases are, however, different.

The plot in fig. 4.5 represents the plot shown in fig. 4.4 on a log-log scale. The trend is same as that found in the case of a two-sphere model.

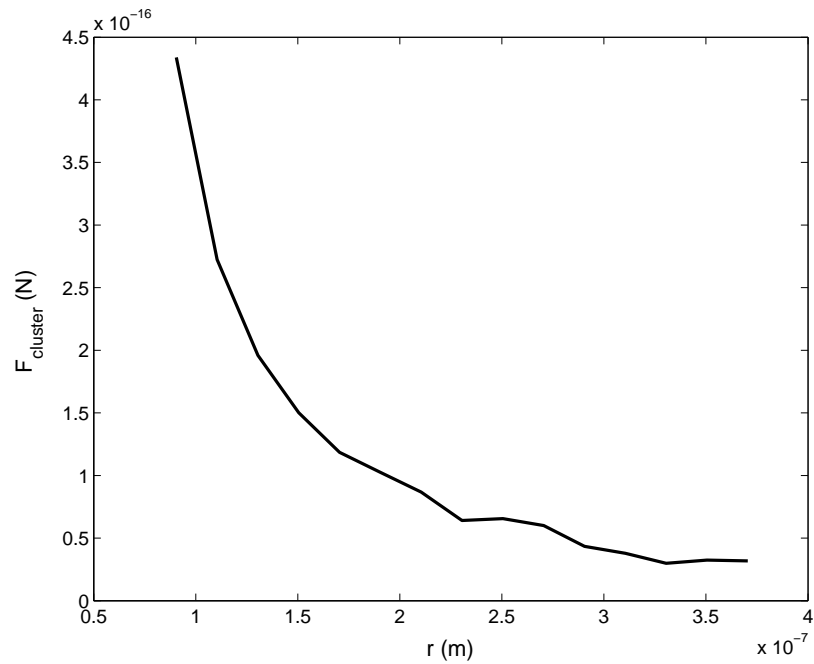


Figure 4.4: Aggregate model – Force vs Distance

Since  $y$  depends on  $r_{12}$ , the separation between the cluster and the sphere 1 at contact, we first define this quantity for the aggregate model.  $r_{12} =$  (the distance between the center of mass of the aggregate and the center of the farthest sphere in the aggregate + the radius of the farthest sphere + the radius of sphere 1). It should be noted that sphere 1 in the simulation need not necessarily be in contact with the farthest sphere when  $r_{12}$  is calculated because its position is chosen at random. The coagulation ratio,  $Z$ , calculated for the aggregate model was observed to be around 1.0010, for a 25 sphere cluster with an individual sphere radius of  $0.01 \mu m$  and a gas temperature of  $1500 K$ .

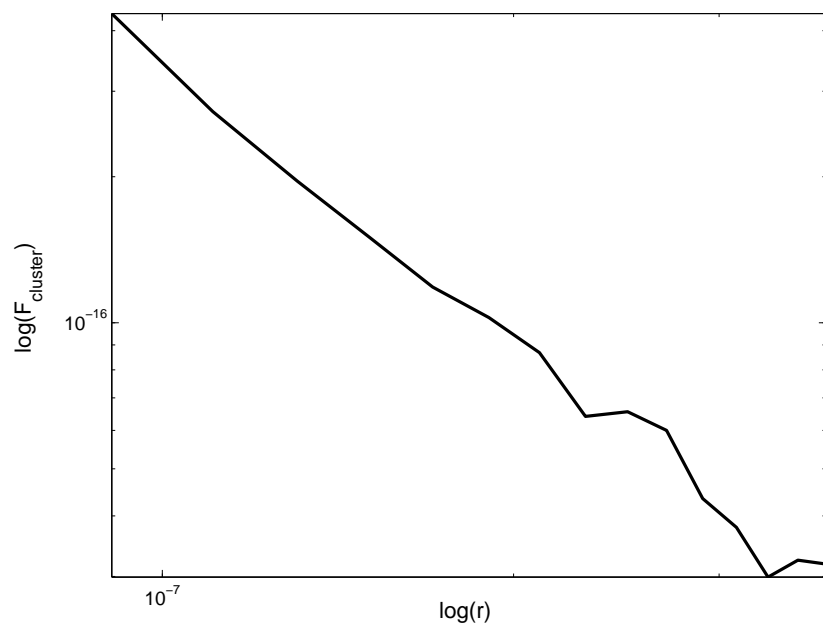


Figure 4.5: Log–Log scale of Fig.4.4

### 4.1.3 Two–sphere equivalent of aggregate model

Table 4.1: Comparison of thermophoretic force magnitudes

$r$	$F_{1-cluster}$	Eq. Volume	Eq. Surface area	Eq. Radius
8.0487	0.3406	0.4802	1.485	3.633
10.0487	0.2397	0.2917	0.916	1.986
12.0487	0.1784	0.2070	0.610	1.321
14.0487	0.1388	0.1521	0.456	0.930
16.0487	0.0994	0.1184	0.346	0.710
18.0487	0.0929	0.0946	0.271	0.557
20.0487	0.0757	0.0753	0.214	0.450
22.0487	0.0559	0.0649	0.180	0.364
24.0487	0.0469	0.0502	0.145	0.303
26.0487	0.0442	0.0421	0.133	0.255
28.0487	0.0369	0.0397	0.118	0.220
30.0487	0.0326	0.0318	0.091	0.186
32.0487	0.0305	0.0290	0.080	0.166
34.0487	0.0272	0.0272	0.073	0.151
36.0487	0.0275	0.0250	0.068	0.142

Table 4.1 shows the comparison of the thermophoretic force,  $F_{1-cluster}$ , in the aggregate model to the thermophoretic force in the two–sphere model when the sphere 2 is replaced with a sphere having (1) equivalent volume, (2) equivalent surface area, and (3) equivalent radius (radius of gyration) as that of the cluster in the aggregate model. The first column ( $r$ ) of the table corresponds to the increasing distance between the centers of the cluster and sphere 1, multiplied by a factor of  $10^{-8}m$ . All values shown in the figure are multiplied by a factor of  $10^{-15}N$ .

#### 4.1.4 Coagulation ratio

Let us first look at the variation of  $y$ , found in the expression for  $Z$ , with  $a$ ,  $T$ , and  $N$  (in the case of aggregates):

$$y \propto N V T^{3.5} r_{12} \left( \frac{G_{1-2}}{F_{1-0}} \right)$$

$$\left( \frac{G_{1-2}}{F_{1-0}} \right) \propto \left( \frac{a^2}{r_{12}^2} \right) \quad \text{and} \quad V \propto a^3$$

$$\Rightarrow y \propto \left( \frac{N a^5 T^{3.5}}{r_{12}} \right)$$

where  $N$  is the number of spheres in the aggregate,  $V$  is the volume of a single sphere,  $T$  is the temperature, and  $r_{12}$  is the separation between the centers at contact.

In the case of two-sphere model,  $N = 1$  and  $r_{12} = 2a$ . Therefore,

$$y \propto a^4 T^{3.5}$$

In the case of the aggregates,

$$r_{12} \propto R_g \propto N^{(\frac{1}{D_f})}$$

$$\Rightarrow y \propto N^{(1-\frac{1}{D_f})} a^4 T^{3.5}$$

Coagulation ratio,  $Z$ , signifies how prominent the thermophoretic force between the particles is, when compared to the Brownian motion alone. It would be an

interesting quantity to look observe at various particle sizes and gas temperatures as in the combustion environments deal a wide range of these parameters.

Table 4.2: Coagulation ratios for various  $a$  and  $T$

$\frac{a \rightarrow}{T \downarrow}$	0.01	0.02	0.03
1500	1.0002	1.0032	1.0163
1800	1.0004	1.00360	1.0304
2000	1.0006	1.0089	1.0461

Shown in Table 4.2 are the coagulation ratios obtained from the two–sphere model for various values of particle sizes ( $\mu m$ ) and gas temperatures ( $K$ ).

Table 4.3: Coagulation ratios for various  $a$  and  $T$

$\frac{a \rightarrow}{T \downarrow}$	0.01	0.02	0.03
1500	1.0008	1.0116	1.0665
1800	1.0013	1.0229	1.1179
2000	1.0021	1.0327	1.1722

Shown in Table 4.3 are the coagulation ratios obtained from the aggregate model for various values of particle sizes ( $\mu m$ ) and gas temperatures ( $K$ ).

## 4.2 Conclusions

A synthetic simulation model has been developed to generate soot targets, and computational molecules and a monte carlo method has been used to calculate (1) the thermophoretic force between cluster–sphere and sphere–sphere configurations, and (2) coagulation ratios. Our results indicate that, at  $a = 0.01 \mu m$  and  $T = 1500 K$ , the coagulation ratio in the two–sphere model is very negligible. However,

the coagulation ratios in the case of an aggregate model could be significant with increasing size of the aggregates (recalling the parameter- $y$  dependency on  $N$ ). It could also be observed, by looking at Table 4.3, that the coagulation ratios for the aggregate model have significantly large magnitudes at larger particle sizes and higher gas temperatures.

Noting the order of increase in magnitude of the coagulation ratios from the two-sphere model to the aggregate model, it could be extrapolated that the effect of radiation on thermophoretic motion of the soot particles would be even more prominent in the case of a cluster-cluster interaction.

The results also show that the sphere aggregates can be approximated by their volume equivalent spheres. We can support the above statement, primarily, by noting that the force scales as the volume of the spheres. However, the magnitude of the force (and hence the comparison to the volume equivalent spheres) in the aggregate model largely depends on the position of sphere 1 relative to the cluster. A lot of work is yet to be done in this aspect to reach to any concluding remarks.

### **4.3 Suggestions for future research**

The future research in the lines of the work presented could involve the dynamic motion of the soot aggregates in the simulation model.

A quasi-random number generator could be used in the monte carlo method implemented instead of the pseudo-random number generator used.

The interaction between a cluster and another cluster could also be an interesting study to carry out taking into account the results presented in the current work for the coagulation ratios of larger-sized particles.



## BIBLIOGRAPHY

- [1] H.F. Calcote. Mechanisms of soot nucleation in flames—a critical review. *Combust. Flame*, 42:215-242, 1981.
- [2] S.J. Harris and A.M. Weiner. Chemical kinetics of soot particle growth. *Annu. Rev. Phys. Chem.*, 36:31-52, 1985.
- [3] Z. Dai, S.S. Krishnan, K.C. Lin, R. Sangras, J.S. Wu, and G.M. Faeth. Mixing and radiation properties of buoyant luminous flame environments. *BFRL Publications*, 1997.
- [4] K.M. Butler and G.W. Mulholland. Generation and transport of smoke components. *Fire Technology*, 40(2):149-176, April 2004.
- [5] T.A. Witten. Diffusion—limited aggregation, a kinetic critical phenomenon. *Phys. Rev. A*, 47:1400-1403, 1981.
- [6] P. Meakin. Diffusion controlled cluster formation in two, three, and four dimensions. *Phys. Rev. A*, 27:604-607, 1983.
- [7] C.M. Sorensen and G.C. Roberts. The prefactor of fractal aggregates. *J. Colloid Interface Sci.*, 186:447-452, 1997.
- [8] F. Zheng. Thermophoresis of spherical and non-spherical particles: a review of theories and experiments. *Adv. Colloid Interface Sci.*, 97:255-278, 2002.
- [9] J.R. Brock. The thermal force in the transition region. *J. Colloid Interface Sci.*, 23:448-452, 1967.
- [10] J.R. Brock. Experiment and theory for the thermal force in the transition region. *J. Colloid Interface Sci.*, 25:392-395, 1967.
- [11] L. Talbot, R.K. Cheng, R.W. Schefer, and D.R. Willis. Thermophoresis of particles in a heated boundary layer. *J. Fluid Mech.*, 101:737-758, 1980.
- [12] G. Zebel. *Aerosol Science*. Academic Press, NY., 1966.
- [13] D.W. Mackowski, M. Tassopoulos, and D.E. Rosner. Effect of Radiative Heat Transfer on the Coagulation Dynamics of Combustion-Generated Particles. *Aerosol Sci. Technol.*, 20(1):83-95, 1994.

- [14] D.W. Mackowski, V. Nayagam, and P.B. Sunderland. Monte–Carlo Simulation of Hydrodynamic Drag and Thermophoresis of Fractal Aggregates of Spheres in the Free–Molecule Flow Regime. *J. Aerosol Sci.*, 2005.
- [15] R.L. Vander Wal. Soot Precursor Material: Spacial Location via Simultaneous LIF–LII Imaging and Characterization via TEM. *NASA Contract Report 198469*, May 1996.

# Appendices

## APPENDIX A

### MONTE CARLO CODE FOR THE TWO-SPHERE MODEL

```
clearall;

l = 1 * power(10, -8);

matrix = [2 * l, 4 * l, 6 * l, 8 * l, 10 * l, 12 * l, 14 * l, 16 * l, 18 * l, 20 * l, 22 * l, 24 * l, 26 *
l, 28 * l, 30 * l];

for initial = 1 : 15,

a = 1 * power(10, -8);

t = 1500;

c = matrix(initial);

theta = acos(2 * rand - 1);

phi = 2 * pi * rand;

xs = 0;

ys = 0;

zs = c;

ni = 0; fx = 0; fy = 0; fz = 0;

n = 50000;

for i = 1 : n,

theta1 = acos(2 * rand - 1);

phi1 = 2 * pi * rand;

theta2 = acos(sqrt(rand));

phi2 = 2 * pi * rand;
```

```

x0 = a * sin(theta1) * cos(phi1);
y0 = a * sin(theta1) * sin(phi1);
z0 = a * cos(theta1);
rs0 = sqrt(abs((xs - x0)).2 + abs((ys - y0)).2 + abs((zs - z0)).2);
u = cos(phi1) * (sin(theta2) * cos(phi2) * cos(theta1) + cos(theta2) * sin(theta1)) -
(sin(phi1) * sin(theta2) * sin(phi2));
v = sin(phi1) * (sin(theta2) * cos(phi2) * cos(theta1) + cos(theta2) * sin(theta1)) +
(cos(phi1) * sin(theta2) * sin(phi2));
w = cos(theta2) * cos(theta1) - (sin(theta2) * cos(phi2) * sin(theta1));
alpha = acos(((xs - x0) * u + (ys - y0) * v + (zs - z0) * w) ./ rs0);
rs = rs0. * sqrt(1 - (cos(alpha)).2);
if cos(alpha) >= 0
if rs <= a
ni = ni + 1;
fx = fx + u;
fy = fy + v;
fz = fz + w;
end
end
end
f12 = ni/n;
fxnet = fx/n;
fynt = fy/n;

```

```

fznet = fz/n;
f = 1 - f12;
gbyf(initial) = abs(fznet/(f));
end
y = -2 * 1.1303 * power(10, 18) * a.^3 * t.^3.5 * gbyf(1) * a
z = (y)./(exp(y) - 1)
force = 2 * 1.5604 * power(10, -5) * a.^3 * t.^4.5 * gbyf
plot(log(matrix), log(force))
figure
plot(matrix, force)

```

## APPENDIX B

### MONTE CARLO CODE FOR THE AGGREGATE MODEL

```
clearall;

a = 1 * power(10, -8);

t = 1500;

no = 20000;

data = xlsread('test4.xls');

nspheres = length(data);

for n = 1 : nspheres,

xs = data(:, 1);

ys = data(:, 2);

zs = data(:, 3);

end

max = 0; kmax = 0;

for k = 1 : nspheres,

r = sqrt(abs(xs(k)).2 + abs(ys(k)).2 + abs(zs(k)).2);

if max == 0

max = r;

kmax = k;

else

if r > max

max = r;
```

```

kmax = k;

end

end

end

for j = 1 : 15,
fall(j) = 0; fxall(j) = 0; fyall(j) = 0; fzall(j) = 0;
end

ctheta = 2 * rand - 1;
stheta = sqrt(1 - ctheta.^2);
phi = 2 * pi * rand;
x11 = stheta * cos(phi);
y11 = stheta * sin(phi);
z11 = ctheta;
for e = 1 : 15,
rmax(e) = max + 2 * e;
x1 = rmax(e) * x11;
y1 = y11 * rmax(e);
z1 = z11 * rmax(e);
y = 1; isamp = 1; err = 1; eps = 0.0005; i = 1;
global mmin;
for m = 1 : nspheres,
f(m) = 0; fx(m) = 0; fy(m) = 0; fz(m) = 0;
end

```



```

i = 1;
isamp = 1; y = 1; err = 1; eps = 0.001;
while i <= no and err > eps,
    ctheta1 = (rand);
    sttheta1 = sqrt(1 - ctheta1.2);
    phi1 = 2 * pi * rand;
    ctheta2 = (sqrt(rand));
    sttheta2 = sqrt(1 - ctheta2.2);
    phi2 = 2 * pi * rand;
    x0 = x1 + sttheta1 * cos(phi1);
    y0 = y1 + sttheta1 * sin(phi1);
    z0 = z1 + ctheta1;
    min = 0; mmin = 0;
    for m = 1 : nspheres,
        rs0 = sqrt(abs((xs(m) - x0)).2 + abs((ys(m) - y0)).2 + abs((zs(m) - z0)).2);
        u = cos(phi1) * (sttheta2 * cos(phi2) * ctheta1 + ctheta2 * sttheta1) - (sin(phi1) *
            sttheta2 * sin(phi2));
        v = sin(phi1) * (sttheta2 * cos(phi2) * ctheta1 + ctheta2 * sttheta1) + (cos(phi1) * sttheta2 *
            sin(phi2));
        w = ctheta2 * ctheta1 - (sttheta2 * cos(phi2) * sttheta1);
        calpha = (((xs(m) - x0). * u + (ys(m) - y0). * v + (zs(m) - z0). * w). / rs0);
        salpha = sqrt(1 - calpha.2);
        rms = rs0 * sqrt(1 - (calpha).2);

```

```

if calpha >= 0
if rms <= 1
sc = rs0. * calpha - (1 - rs0.^2. * salpha.^2).^(1/2);
if min == 0
min = sc;
mmin = m;
umin = u;
vmin = v;
wmin = w;
else
if sc < min
min = sc;
mmin = m;
umin = u;
vmin = v;
wmin = w;
end
end
end
end
end
if (mmin = 0)
f(mmin) = f(mmin) + 1;

```

```

fall(e) = fall(e) + 1;
fx(mmin) = fx(mmin) + umin;
fy(mmin) = fy(mmin) + vmin;
fz(mmin) = fz(mmin) + wmin;
fxall(e) = fxall(e) + umin;
fyall(e) = fyall(e) + vmin;
fzall(e) = fzall(e) + wmin;
end
if (mod(i,100) == 0)
samp(y) = fall(e)./i;
y = y + 1;
holdon;
end
if (floor(i/100)) >= 10 and mod(i,100) == 0,
fsamp = samp(isamp : (isamp + 9));
isamp = isamp + 1;
if mean(fsamp) = 0
err = std(fsamp)./mean(fsamp);
actual = i;
end
end
i = i + 1;
end

```

```

f = f./actual;
fall(e) = fall(e)./actual;
fxnet = fx./actual;
fynet = fy./actual;
fznet = fz./actual; fxnetall(e) = fxall(e)./actual;
fynetall(e) = fyall(e)./actual;
fznetall(e) = fzall(e)./actual;
fnet = sqrt(fxnet.2 + fynet.2 + fznet.2);
fnetall(e) = sqrt(fxnetall(e).2 + fynetall(e).2 + fznetall(e).2);
gbyf = abs(fnet/(1 - f));
gbyfall(e) = abs(fnetall(e)/(1 - fall(e)));
c = sqrt(abs(x1 - xs).2 + abs(y1 - ys).2 + abs(z1 - zs).2) * power(10, -8);
yc = -2 * 1.1303 * power(10, 18) * a.3 * t.(3.5) * gbyf * c;
ycall = -2 * 1.1303 * power(10, 18) * a.3 * t.(3.5) * gbyfall(1) * rmax(1) * a;
z = (yc)./(exp(yc) - 1);
zall = (ycall)./(exp(ycall) - 1)
force = 2 * 1.5604 * power(10, -5) * a.3 * t.(4.5) * gbyf;
forceall(e) = 2 * 1.5604 * power(10, -5) * a.3 * t.(4.5) * gbyfall(e)
end
plot(rmax, forceall)
figure
plot(log(rmax), log(forceall))

```